



Shoreline Evolution Between Al Lith and Ras Mahāsin on the Red Sea Coast, Saudi Arabia Using GIS and DSAS Techniques

Aaid G. Al-Zubieri^{1,3}  · Ibrahim M. Ghandour^{1,2} · Rashad A. Bantan¹ · Ali S. Basaham¹

Received: 17 February 2020 / Accepted: 3 September 2020 / Published online: 19 September 2020
© Indian Society of Remote Sensing 2020

Abstract

A large proportion of the world's population lives in coastal areas. These zones play a vital role in the socioeconomic aspects of coastal communities. The evolution of shoreline along the zones is of great importance to scientists, and engineers as well as coastal management. This research aims to assess and understand the dynamics of shoreline along the Red Sea coast between Al Lith and Ras Mahāsin, using medium-resolution satellite imagery over 34 years (1984–2018) as well as to predict futuristic changes in the shoreline position until 2038. The tasseled cap transformation tools in ArcGIS 10.2 are used to extract shoreline position for seventh intervals time. These shorelines are analyzed by the digital shoreline analysis system in four statistical functions, namely (EPR, LRR, NSM, and LMS). The endpoint rate is used to predict futuristic shoreline positions. The results reveal that the evolutions of shoreline in the form of erosion and accretion patterns, as surface area exceed 12.3 and 0.89 km², respectively. The evolution rates were classified based on LRR into five classes: [i.e., – 11.84 to – 7.85 (very high erosion), – 7.85 to – 4.17 (moderate erosion), – 4.17 to 0.00 (low erosion), 0.00 to 1.28 (low accretion), and 1.280 to 14.44 (high accretion)]. These changes are attributed to the impact of the extreme wave action and the littoral drifts of sediments by longshore currents. The prediction model reveals that a large portion of the coastal zone is vulnerable to a high rate of shoreline disintegration.

Keywords Shoreline evolution · DSAS · Endpoint rate · Linear regression rate · Red Sea

Introduction

Coastal zones are socially and economically growing areas that are inhabited by millions of people. These zones are affected by the coastal accretion, erosion, sediment transportation, sediment redistribution, environmental intervention, human intervention, and coastal evolution modifying in long- and short-term scales (Boak and Turner 2005; Holland and Elmore 2008; Aedla et al. 2015; Castelle et al. 2018; Rabehi et al. 2019; Shetty et al. 2019;

Vousdoukas et al. 2020). The coastal degradation impacts ways of living, possessions, protection of harbors, environmental, and socioeconomic aspects as well as coastal and land resources. Therefore, monitoring and evolution of shorelines along the zones are of great importance to coastal communities, scientists, and engineers as well as coastal management. The shoreline is defined as the land–water interface which is an exceptionally unique component, raising indicators for coastal disintegration and accretion (Genz et al. 2007). Traditionally, the position of the shoreline is extracted from aerial photography by several authors (Boak and Turner 2005; Pianca et al. 2015) as a line visible to the analyzer's eye. Recently, quite a few automatic shoreline extraction techniques have been suggested a comparison of two independent land cover classifications, and density slice using single or multiple bands. The most recent technique is tasselled cap transformation (TCT), proposed by (Pardo-Pascual et al. 2012), and used by coupling geographic information system (GIS) with digital shoreline analysis system (DSAS) (Thieler et al.

✉ Aaid G. Al-Zubieri
aahmed0217@stu.kau.edu.sa

¹ Marine Geology Department, Faculty of Marine Sciences, King Abdulaziz University, P.O. Box 80200, Jeddah 21589, Saudi Arabia

² Department of Geology, Faculty of Science, Tanta University, Tanta 31527, Egypt

³ Department of Marine Geology, Faculty of Marine Sciences, Hodeidah University, Hodeidah, Yemen

2009; Baral et al. 2018; Hagenaaers et al. 2018; Nassar et al. 2018; Ciritci and Türk 2019). The authors suggested that the technique is more accurate due to its least standardized root-mean-square mistakes with related field information.

Globally, qualitative and quantitative analysis of shoreline evolution predicts future positions of shoreline to relieve the impact of forthcoming disintegration processes that have gained prominence by several authors (Addo et al. 2008, 2012; Tran Thi et al. 2014; Kabuth et al. 2014; Murali et al. 2015; Pianca et al. 2015; El-Sharnouby et al. 2015; Nandi et al. 2016; Almonacid-Caballer et al. 2016; Bheeroo et al. 2016; Jonah et al. 2016; Nassar et al. 2018; Qiao et al. 2018; San and Ulusar 2018; Zhang et al. 2018; Castelle et al. 2018; Fan et al. 2018; Ciritci and Turk 2020). These studies elucidated that integrating GIS and DSAS can be effectively used to assess temporal shoreline evolution.

Territorially, few motivational studies carried out along the Red Sea coast. Bantan (1999) processed Landsat TM image variably to examine the surface geology of the Farasan Islands as palaeo-bathymetry and recent sedimentology. Alharbi et al. (2011) used Landsat imagery to identify coastal landforms. Nofal and Abboud (2016) maintained that the circumstances forming geomorphological features on the eastern coast of the Red Sea in Saudi Arabia are not permanent since it changes rapidly and continuously due to erosion and uplifting processes. Alharbi et al. (2017) reported that there are massive changes in the temporal shoreline along the southern Red Sea coast of Saudi Arabia recorded at the maximum accretion of 36.4 m and maximum erosion at 12.9 m. These changes are linked to infrastructure developments. Al-zubieri et al. (2018) indicated that there is a shrink in the tidal flat in front of the Jazan coast due to the effect of socioeconomic activities during the last decade. Aboulela et al. (2020) studied the evaluation of the coastlines of Jeddah City using satellite images for the period from 1972 to 2016. The authors found witnessed reduction in the surface area along the coast, which probably due to various anthropogenic activities. Since 1973, there is a shortage of detailed studies on the dataset of satellite imagery by using GIS and DSAS techniques, particularly between Al Lith and Ras Mahāsin along the Red Sea coast in Saudi Arabia to monitor shoreline evolution and prediction models for future changes.

On the other hand, the coastal zone of the Red Sea is characterized by numerous geomorphological features like shallow tidal flats, distributary channels of Wadies, Sabkhas, Sharm, Khors, and lagoons. It is also joined to the Indian Ocean through the Straits of Bab al-Mandab, which replenish waters with a unique water exchange processes. Therefore, it needs more attention to monitor and execute coastal zone management policies more effectively. The

present study aims to assess and understand the dynamics of shoreline evolution between Al Lith and Ras Mahāsin along the Red Sea coast of Saudi Arabia using GIS and DSAS techniques as well as predicting futuristic changes in the shoreline positions using EPR model. Additionally, we intend to provide a system of proposals for the current situation to enable decision-makers to illuminate the incidental issues along the Red Sea Coast.

Study Area

The study area is situated between latitude 19° 32.576' N and 20° 9.496' N and longitude 40° 54.453' E and 40° 14.157' E with the length of 150 km, extending between Al Lith to Ras Mahāsin near Al Qunfudhah beaches in the middle part of the Red Sea coast (Fig. 1). Various features currently exist in this area (e.g., Marine heads (Ras Mahāsin and Ra's Kinnateis), Ghubbat al Mahasin, Sabkha, Mangroves, Wadies mouth, and Strand plain. Climatically, the investigated area falls under tropical monsoon climate type with warm and dry conditions staying through the year. Generally, the temperature gradient varies from (29°–38.5 °C) and (21°–30 °C) during spring and winter, respectively. In the last decade, humidity record was fluctuating between 6 and 68%, sometimes reached to a maximum of 100%. The mean monthly rainfall is scarce (63 mm per year) with intermittent wadi channels inflow. The highest noteworthy precipitation occurs during rainstorms (October to May), and the mean breeze speed recorded around 12 km/h by (AL-Sheikh 2012). On the other ways, it sites at the boundary of northward and southward shifting of the intertropical convergence zone (ITCZ) (Edwards 1987; Abu-Zied and Bantan 2015). This setting makes it an ideal location for shoreline evolution. From June to September, the Red Sea subjects to the winds flowing from the northwest, while from October to May, the winds become two-directional. The first direction is coming from southeast passing through the Strait of Bab el Mandeb to reach about 19°N while the second is flowing from the northwest to cover the northern part of the Red Sea (Murray and Johns 1997; Siddall et al. 2003).

The patterns of the winds oriented along the axis of the Red Sea make variability of waves in this area through summer and winter. During the summer, the winds blow from the northwest over the Red Sea, generating small waves that reach the area. These waves sometimes are enhanced by a mountain wind jet from the Tokar Gap to exceed monthly mean 2 m with the power reaching up to (1.7 kW/m) along the coast. However, monsoon winds from the southeast over the Red Sea, generating relatively high waves exceed 2 m at the mean periods of 8 s in the area of study with the highest average wave power

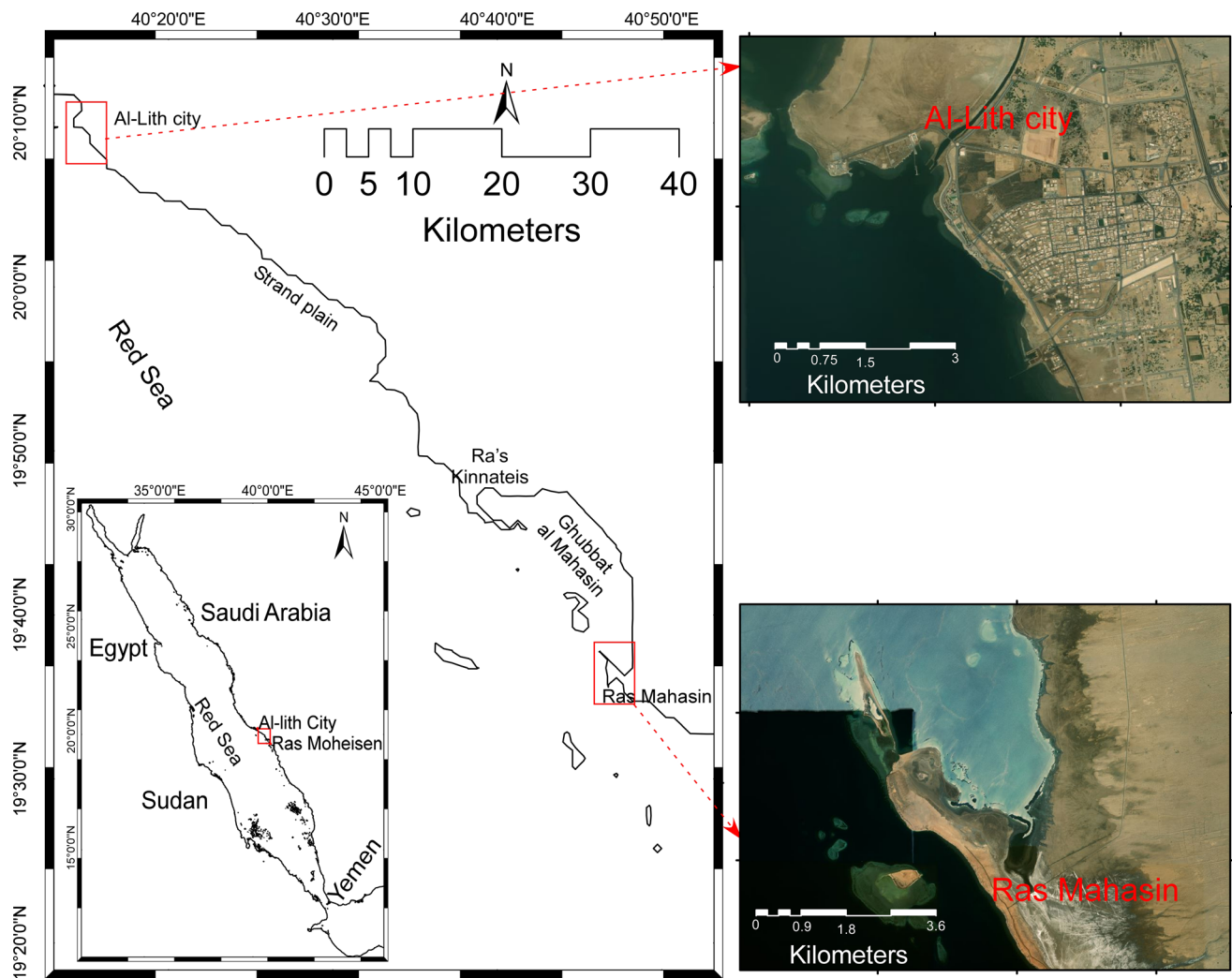


Fig. 1 Simplified map showing the area of study

reaching up to 6.5 kW/m along the coast (Ralston et al. 2013; Aboobacker et al. 2017). The geostrophic currents along the coast of the investigation area flow northward and southward, which are modified in the presence of cyclonic and anticyclonic eddies. During summer, the anticyclonic eddies occur on the west coast of the Red Sea while the cyclonic eddies occur on the east coast of the Red Sea. However, the cyclonic eddies are in the reversed pattern during winter (Taqi et al. 2019). The annual variance of mean tide ranges from 0.4 to 0.8 m. The amplitudes of both diurnal and semidiurnal constituents' tidal currents ranged from 0.1 to 1 m (2013). They confirmed the occurrences of the anticlockwise amphidromic system in this part of the Red Sea (Gharbi et al. 2018). The low tidal range causes sabkha immersion by a thin dainty sheet of water as opposed to through a system of channels (Behairy et al. 1991). During the winter, the average sea level was usually higher than the average in summer, and tidal speeds affected by choking influences brought about by

reefs, sand bars, and low islands, regularly surpass $1\text{--}2 \text{ m s}^{-1}$.

Eight satellite images spreading over a 34-year time span (1984–2018) were taken into consideration. Medium-resolution satellite data such as Landsat TM and ETM+ were used for shoreline evolution in the study area. The satellite datasets were gathered at irregular intervals due to the inaccessibility of cloud-free imagery during the chosen period. The details of the satellite dataset, acquisition details, and resolutions are presented in Table 1.

Methodology

The methodological framework applied in the study can be divided into three sections. The first section deals with data processing such as Image co-registration, radiometric correction, and enhancement using ENVI software. The second section extracts shoreline position for seven intervals

Table 1 Details of satellite dataset (acquired via <https://eos.com/landviewer/> and <https://earthexplorer.usgs.gov/>)

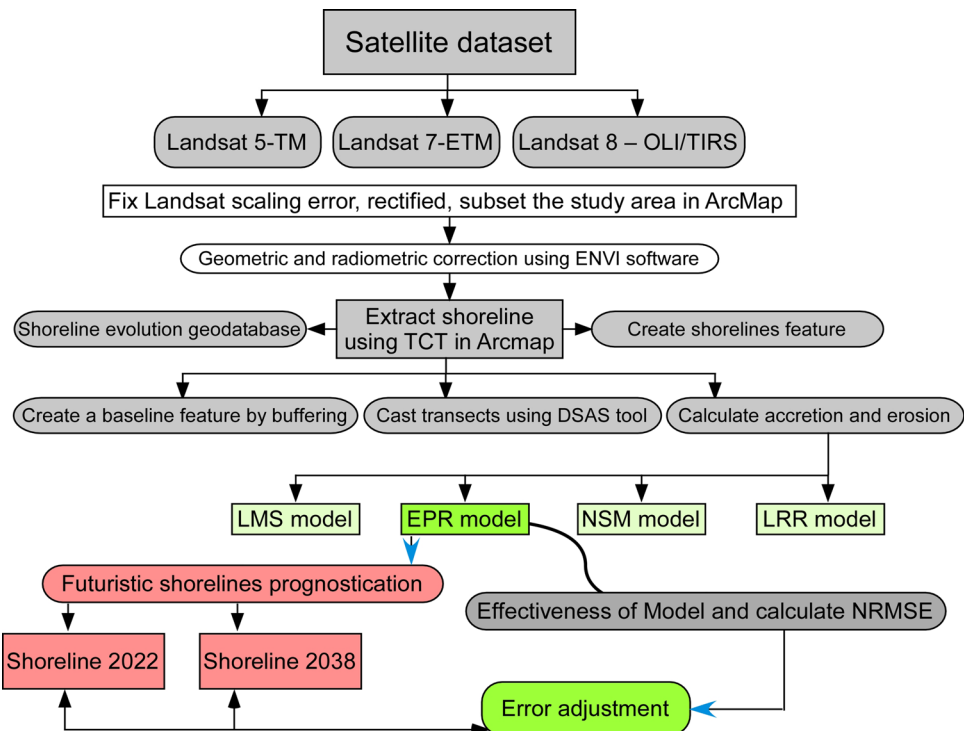
Satellite data	Path/row	Acquisition year	Pixel resolution (m)
Landsat 5—TM	169/46	17/07/1984	30
Landsat 5—TM	169/46	21/06/1986	30
Landsat 5—TM	169/46	16/06/1990	30
Landsat 5—TM	169/46	27/06/1994	30
Landsat 5—TM	169/46	22/06/1998	30
Landsat 7—ETM+	169/46	10/06/2014	30
Landsat 7—ETM+	169/46	02/06/2017	30
Landsat 7—ETM+	169/46	05/06/2018	30

1984, 1986, 1990, 1994, 1998, 2014, and 2018 using TCT (Pardo-Pascual et al. 2012) and different processes of spatial analysis using ArcGIS 10.2 package. The third section dealing with the evolution of shoreline in the form of accretion/erosion fashions was estimated using three statistical approaches in DSAS, namely endpoint rate (EPR), movement of shoreline (NSM), and linear regression rate (LRR). The EPR is used to predict futuristic changes in the shoreline positions following the techniques used by (Nassar et al. 2018). The methodological structure is summarized in the flowchart (Fig. 2), and a detailed explanation is presented in the following sections.

Data Processing and Shoreline Extraction

A Landsat (TM and ETM+) for the period between 1984 and 2018 with irregular intervals were downloaded from eos.com/land viewer. The datasets are radiometric corrected by ENVI software and rectified using geo-referenced tools in the ArcMap package. The rectifying was performed based on eleven ground control points, selected carefully at the landmarks on the high-resolution image of Google Earth and WGS-84 datum. The rectifying accuracy of the selected points was 0.276 pixels of root-mean-square error (RMSE). The RMSE is the squared difference between dataset coordinate values and coordinates from an independent source of higher accuracy for identical points (Maanan et al. 2014). The images of the selected area were extracted using the mask of raster processing in ArcMap.

Fig. 2 Methodology flowchart



The subset images were exported to ENVI software to perform the radiometric correction again to avoid the effect of extraction processing. This correction is based on the information such as offset/gain, sun elevation, and satellite viewing angles, which were available in the Landsat metadata documentation. The next step is to extract shoreline, using TCT. The TCT is a technique which reclassifies spectral information of the six ETM+ bands into three principal view components (i.e., brightness, greenness, and wetness) through the coefficients derived by sampling known as the land cover spectral characteristics (Huang et al. 2002; Pardo-Pascual et al. 2012). These components with NDVI were used to create categories, which were reclassified into two classes, namely land and sea. The shoreline was extracted for every interval (Fig. 3).

The Estimate of Shoreline Evolution

Shorelines were analyzed using the DSAS technique, which is developed by the United States Geological Survey (USGS). These analyses were based on baseline features at systemic transects that cut the shorelines every 20 m and numbered from south to north (Fig. 4). The evolution of shoreline in the form shape of accretion/erosion patterns was estimated using four statistical approaches in DSAS, namely endpoint rate (EPR), net shoreline movement, linear regression rate (LRR), and least median of squares. The EPR is used to predict futuristic changes in the shoreline positions following the equation proposed by (Fenster et al. 1993) and recently assured as a trustworthy tool by several authors (Mukhopadhyay et al. 2012; Nandi et al. 2016; Mondal et al. 2017; Nassar et al. 2018). In the present study, this equation was performed based on the historical shoreline of 1984 and 2018 in the following expression.

$$P_{t'} = P_L + m_{\text{EPR}} * (t' - T_L) \quad (1)$$

where P_L is the position of shoreline at the last time 2018 (T_L), $P_{t'}$ is the future shoreline position at a specific time (t'), and m_{EPR} is the rate of shoreline change (EPR) between 1984 and 2018.

On the other hand, the effectiveness of predicted shorelines was validated in terms of the normalization of root-mean-square error (NRMSE) as per the following expressions.

$$\text{RMSE} = \sqrt{\sum_i^n (L_{\text{exs_}Y,i} - L_{\text{Prds_}Y,i})^2 / n} \quad (2)$$

$$\text{NRMSE} = \text{RMSE} / L^{-\text{alex_}Y} \quad (3)$$

where n is transecting numbers; $L_{\text{exs_}Y,i}$ is the remoteness between baseline and the extracted shoreline for 1998 and

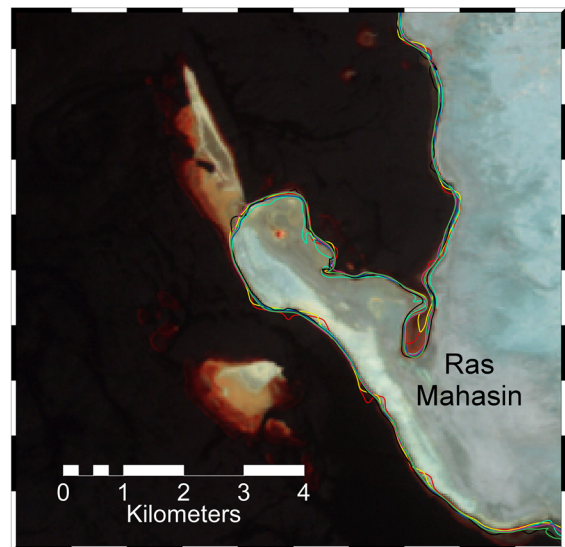
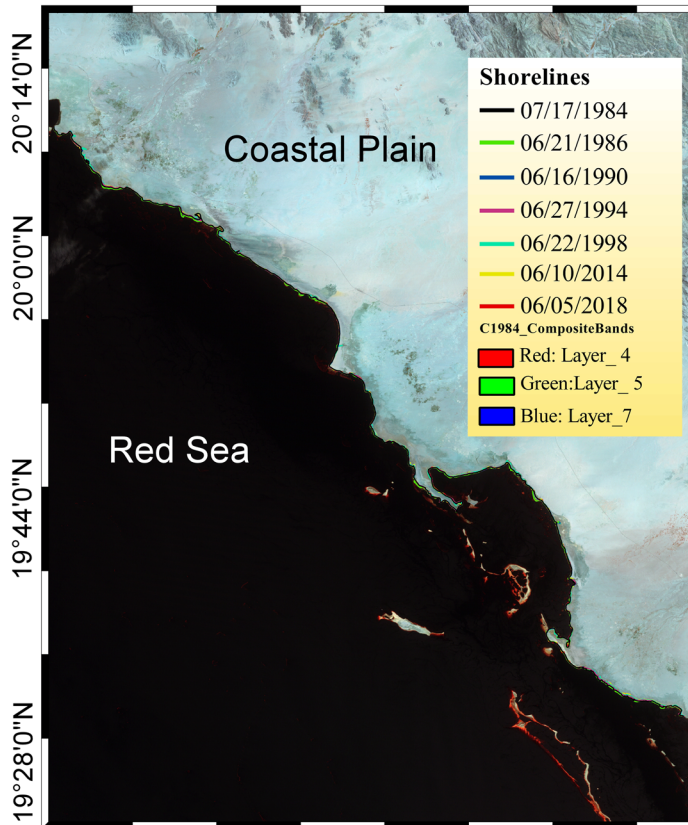
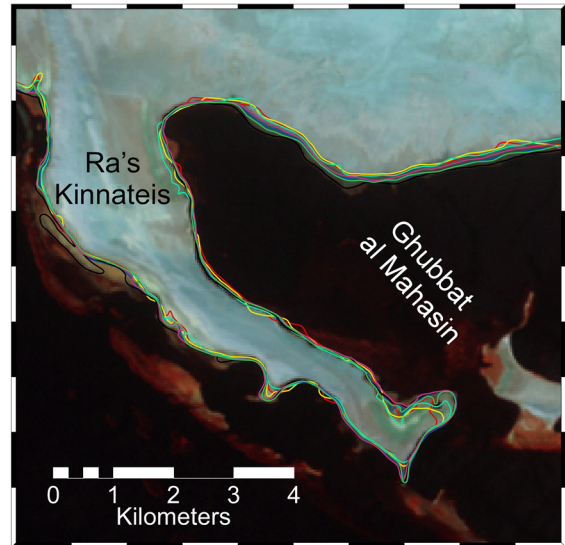
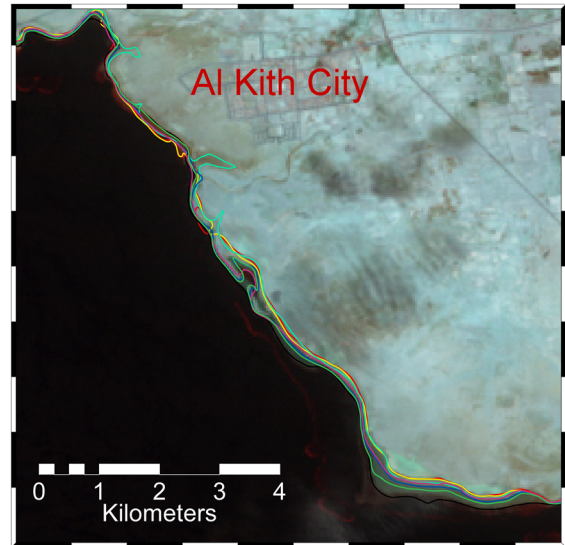
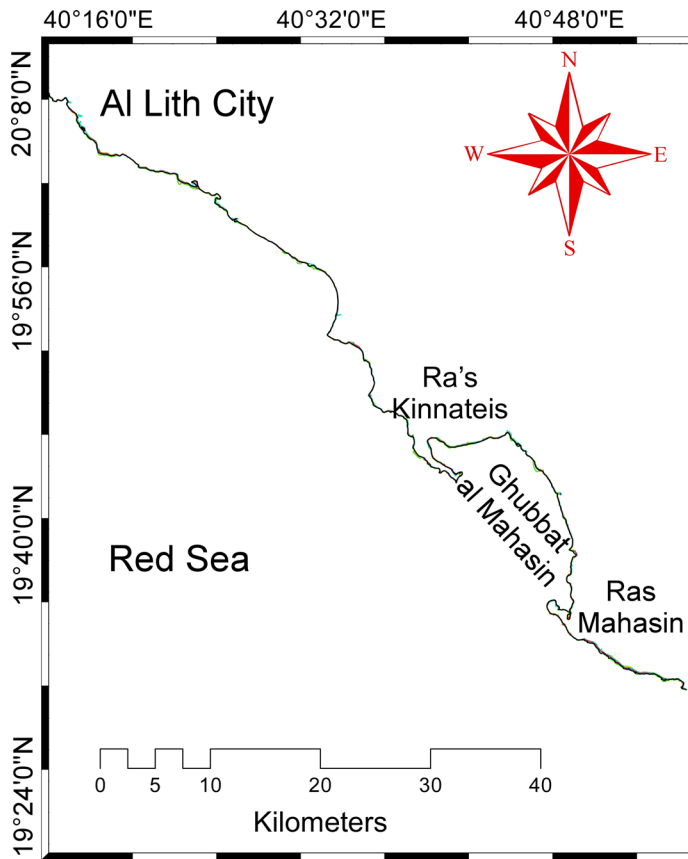
2017 at transect number i ; $L_{\text{Prds_}Y,i}$ is the remoteness between baseline and the predicted shoreline for 1998 and 2017 at transect number i ; and $L^{-\text{alex_}Y}$ is the mean of the remoteness of the extracted shoreline for 1998 and 2017.

Results and Discussion

Shoreline Evolution

Two-dimensional shoreline evolution identification was widely researched along the coastal zone between Al Lith and Ras Mahāsin on the Red Sea coast over 34 years with irregular period intervals (1984, 1986, 1990, 1994, 1998, 2014, and 2018). This procedure was actualized through a lot of substantial steps, as shown in Fig. 2. The total erosion/accretion was calculated during the time of 1984–2018 (Fig. 5). As shown in Figs. 5 and 6, the shoreline evolution during the studying period revealed that the study area exhibited a huge shoreline erosion and accretion. The amplitude of both of them exceeded 12.3 and 0.89 km², respectively. These evolutions were occurring along the coastal zone from south to north, and the most significant changes were recorded at marine heads like Ras Mahāsin and Ra's Kinnateis (Fig. 5). These marine heads appeared in the shape of a semi-crescent shape, emerges from the land toward the sea, making them more vulnerable to the effect of wave action. Coastal processing such as the power of wave energy, longshore current with the contribution of tidal currents, probably reformed geomorphology of these heads. Similarly, Nofal and Abboud (2016) found high erosion on the marine head of the Ras Al-Shabaan on the Northern Red Sea coast. They interpreted increasing erosion at this marine head to the effect of wave movements and current endings.

While the erosion on other portions of shoreline in the south is attributed to the consolidated activity of combined impacts of the stormy climate of the coast and restricting sediment movements, coming from wadi channels in landward. This transportation of sediment along the coast was carried out by waves action and longshore currents that induced within the breaker zone (May and Hansom 2003). In the light of hydrodynamic conditions in this portion of the coast, alongshore flows have derived dismantled sediments from south to north, leaving a much disintegrated zone. This may occur due to the high power of waves energy along the coast of this portion due to the parts falling within the intertropical convergence zone (ITCZ) and faces open sea waves directly (Ralston et al. 2013; Aboobacker et al. 2017). Aboobacker et al. (2017) mentioned that the power of wave energy along the coast of this part of the Red Sea reached up to 6.5 kW/m. However,



◀ **Fig. 3** Shorelines extraction with false-color composite images for all studied intervals

severe accretion has occurred on the northern portion of shoreline near Al Lith City, where human intervention became extensively active, leading to more significant accretion. Furthermore, dynamic and broad growth occurred in and around this area, as Al Lith City expanded on seaward.

Application of DSAS

The DSAS technique is applied to calculate the rate of evolution statistically from seven historical shoreline positions, starting from June 1984 to June 2018 between Al

Lith and Ras Mahāsin on the Red Sea coast. The processes of this technique are summarized in Fig. 2. A qualitative analysis was performed to determine erosion/accretion transects utilizing EPR and LRR models in the study area (Fig. 6a, b). The output of shoreline evolution rates was spatially evaluated for the study area through all the period using statistical functions of linear regression and endpoint rates with significant correlation $r^2 = 0.85$ (Fig. 6b). The positive values above the zero line in Fig. 6a indicate accretion, while the negative values beneath the zero line reveal erosion.

The LRR outputs are classified into five class: (− 11.84 to − 7.85: very high erosion), (− 7.85 to − 4.17: moderate erosion), (− 4.17 to 0.00: low erosion), (0.00 to 1.28: low accretion), and (1.280 to 14.44: high accretion) to represent the risk levels along the study area. This classification was

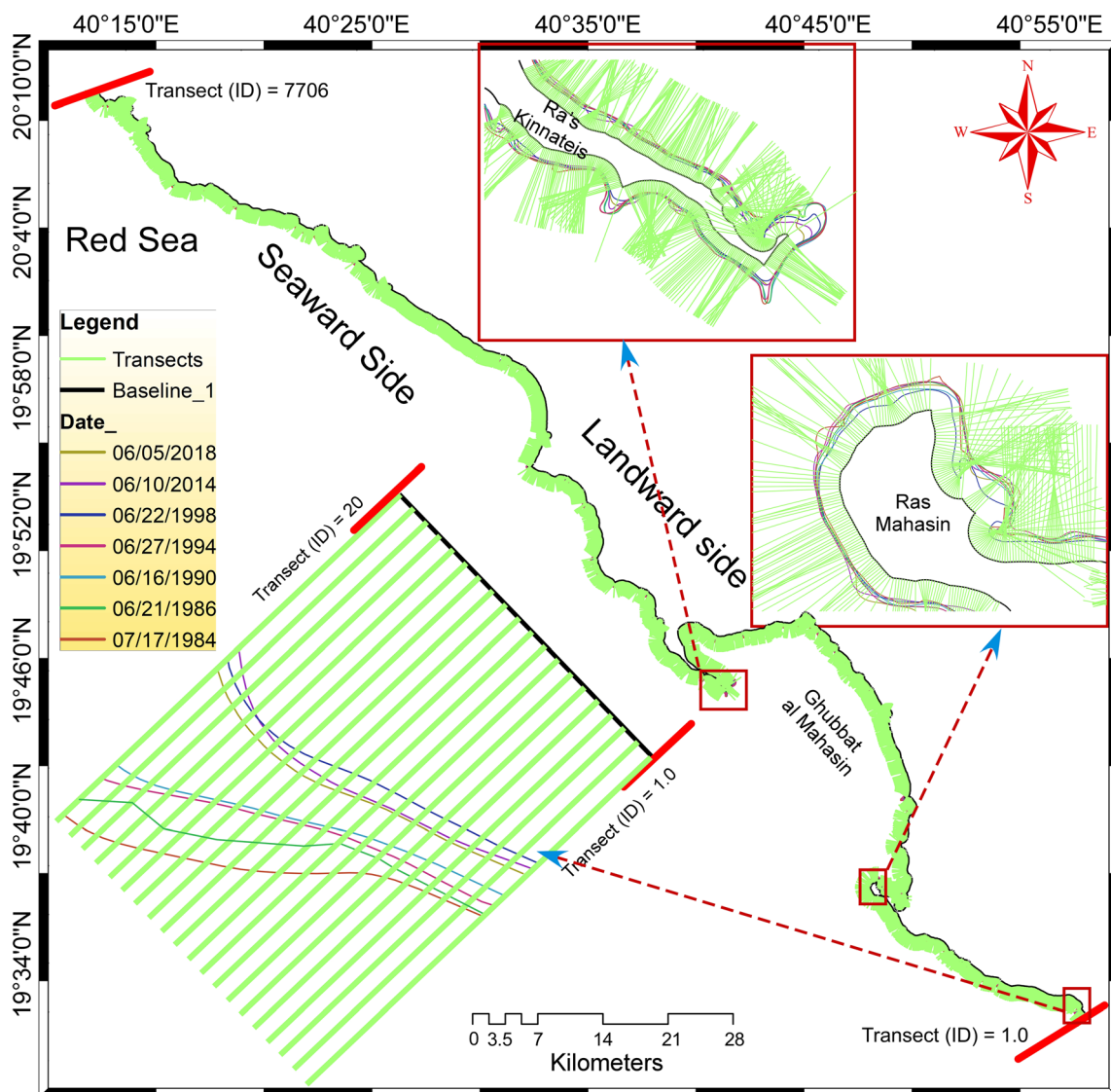


Fig. 4 Systemic transects from baseline in the landward side, which cut the shorelines every 20 m using DSAS

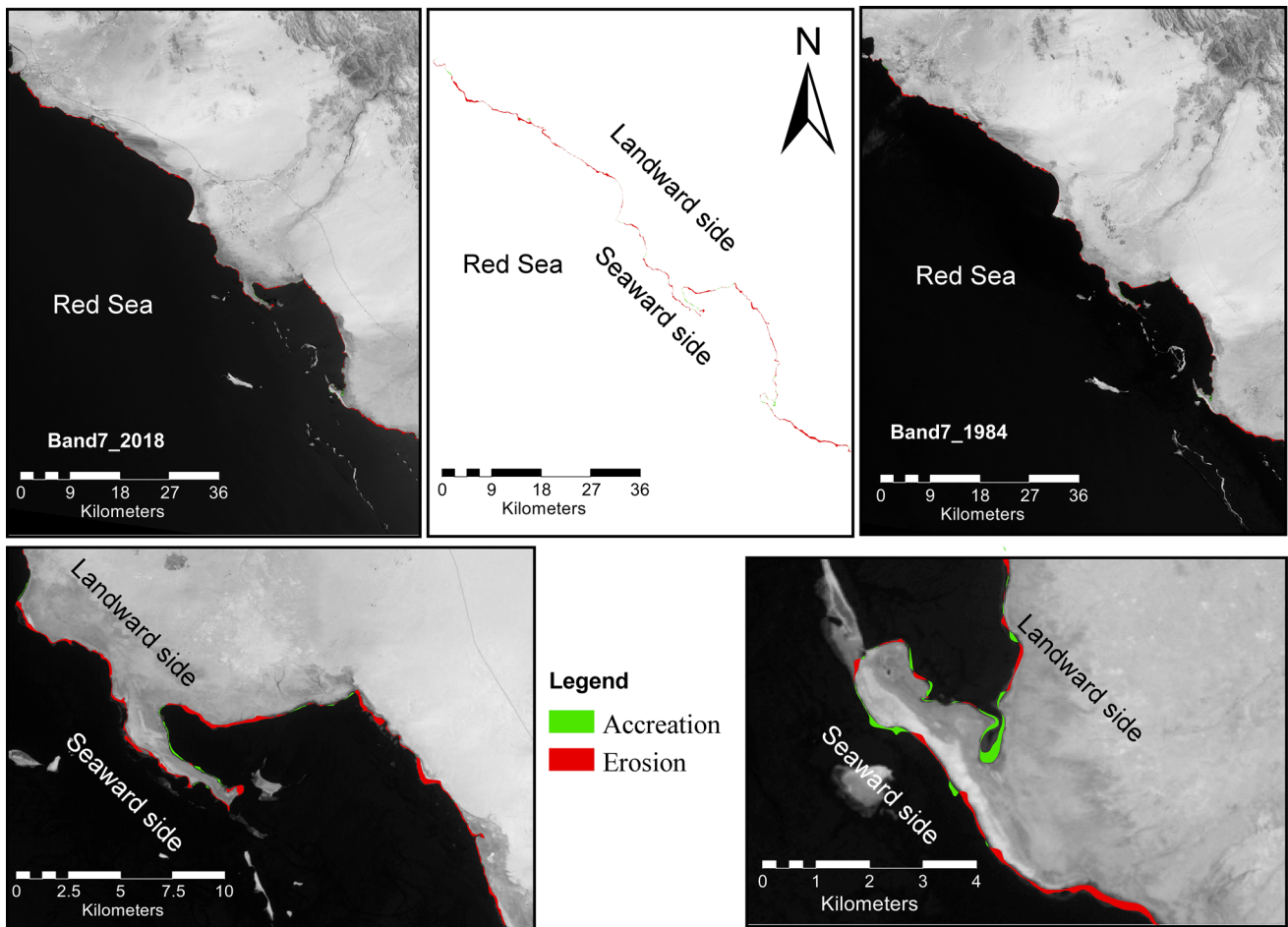


Fig. 5 Erosion and accretion along the studying area between 1984 and 2018

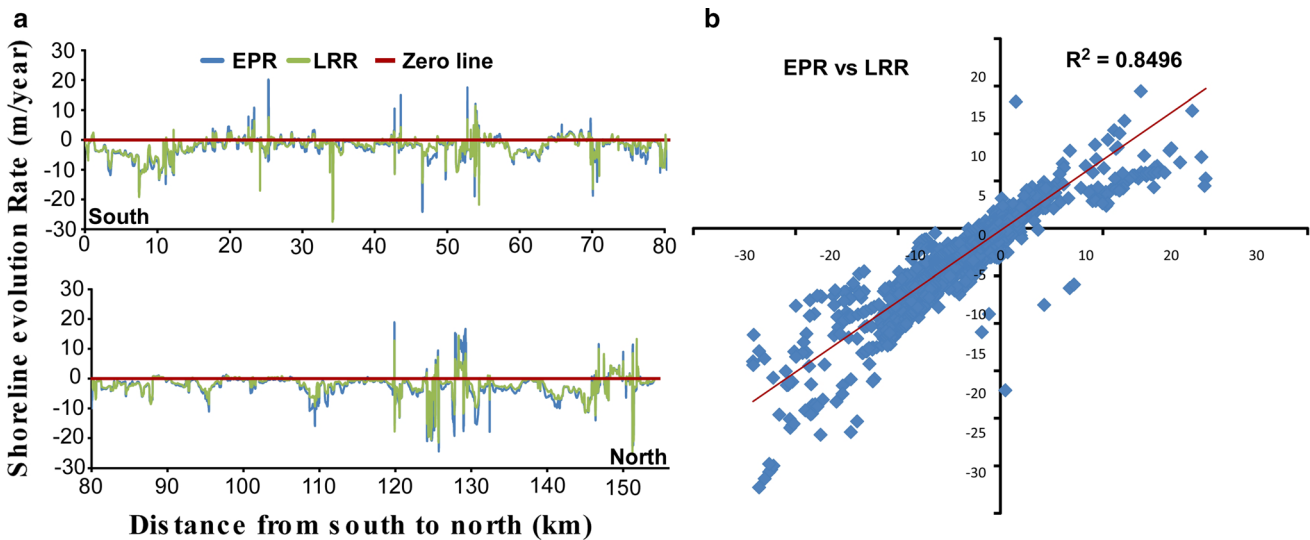


Fig. 6 a) Shoreline evolution rate by LRR and EPR during the interval between 1984 and 2018, and b) Correlation between LRR and EPR statistical functions overall the stud area

carried out based on the potential socio-environmental losses and the criteria of coastal vulnerability, as defined by

Mahapatra et al. (2014, 2015). The risk levels could help decision-makers in the management of coastal areas of

Saudi Arabia to reduce impacts of erosion and construction and to take proper system toward existing seaside issues along with the investigation area. Depending on this classification, the shoreline evolution was plotted against LRR values as three portions. The first portion explains shoreline evolution along with the southern sector around Ras Mahāsin (Fig. 7). It illustrates that most of this sector is subjected to erosion processes, exhibiting very high erosion in its southern part. A maximum erosion rate of -20 m/year takes place between latitudes ($19^{\circ} 32'$ and $19^{\circ} 36'$). Subsequently, the littoral eroding was dragged out toward the marine head of Ras Mahāsin, paying by northward longshore currents, interfused with a maximum rate of 12 m/year and situated along with the marine head. This means that the shoreline in this part was more dynamically and vulnerably against the high rate of shoreline disintegration. Accordingly, this part of the coast needs more attention to protect regulations, such as the construction of a wave breaker zone in a remote area in the open sea.

The second portion explains shorelines evolution along Ghubbat al Mahasin and Ra’s Kinnateis (Fig. 8). It has shown that the shoreline at this zone has, in general, moderate erosion along with the most places of shore on Ghubbat al Mahasin and low accretion along with the marine head of Ra’s Kinnateis on the side of Ghubbat al

Mahasin. The low erosion took place along the marine head on the open seaside. Furthermore, unsymmetrical mean shore evolution rates based on LRR were recorded between 5 and -10 m/year along the coast of Ghubbat al Mahasin. This unsymmetrical evolution inside the Ghubbat al Mahasin was due to the geomorphological shape of Ghubbat al Mahasin and based the energy of the waves that come from the open sea by the narrow inlets between small islands which available at the Ghubbat al Mahasin entrance. Whereas, maximum erosion along Ra’s Kinnateis coast on open seaward was -12 m/year may be due to the effect of wave action.

Figure 9 describes the accretion/erosion between Al Lith and Ra’s Kinnateis. The amplitude of accretion in this portion was higher than in other sectors. This accretion is attributed to socio-environmental activities as human intervention became extensively active, leading to more significant accretion. Furthermore, dynamic and broad growth in and around this area occurred as the expansion of Al Lith City on seaward. Additionally, the erosion rate in this sector ranged from less than -5 m/year (low erosion) to 25 m/year (high erosion). This erosion has been continuing northwards from Ra’s Kinnateis shore at a distance of 40 km to reach near Al Lith shore, indicating more dynamics of shoreline, needing more attention, and putting

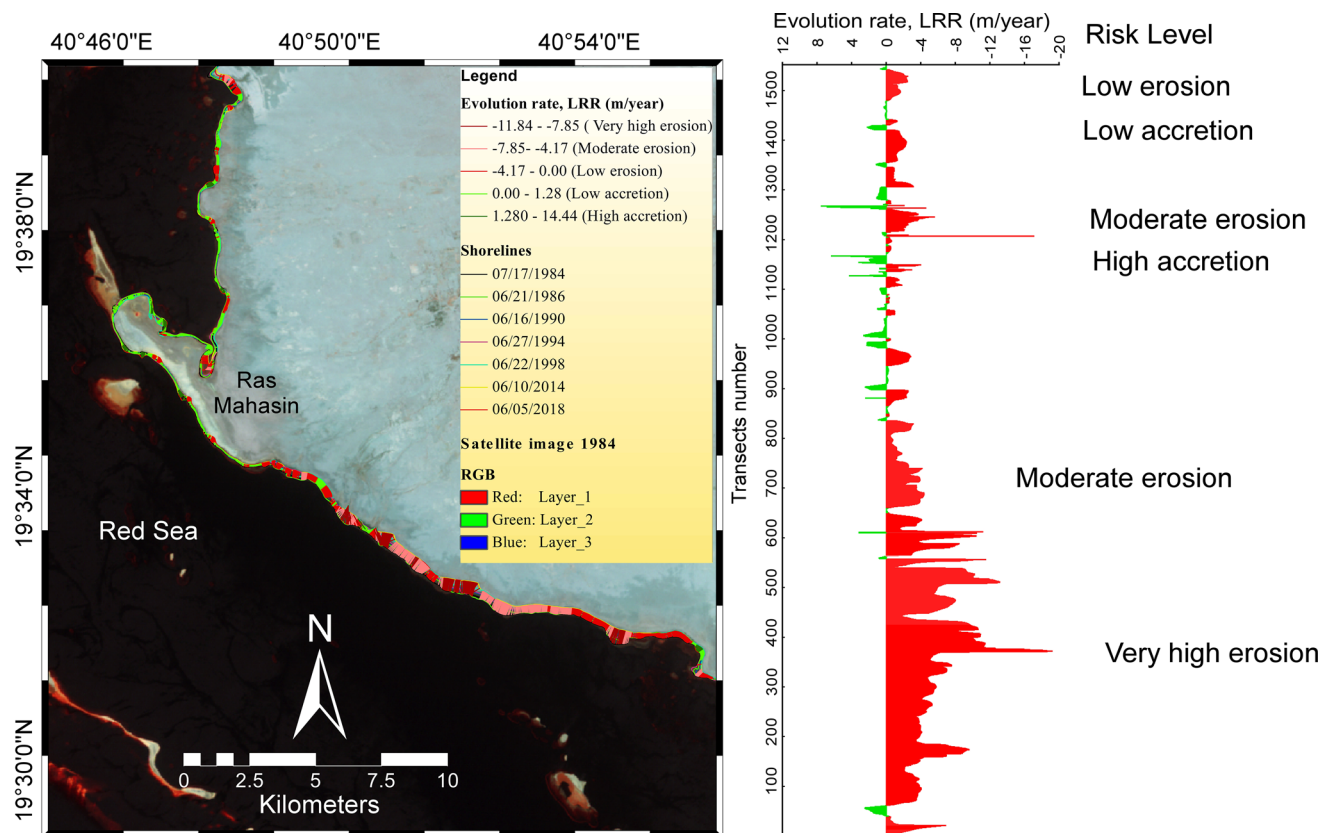


Fig. 7 Assessments of shorelines evolution along with the southern sector around Ras Mahāsin

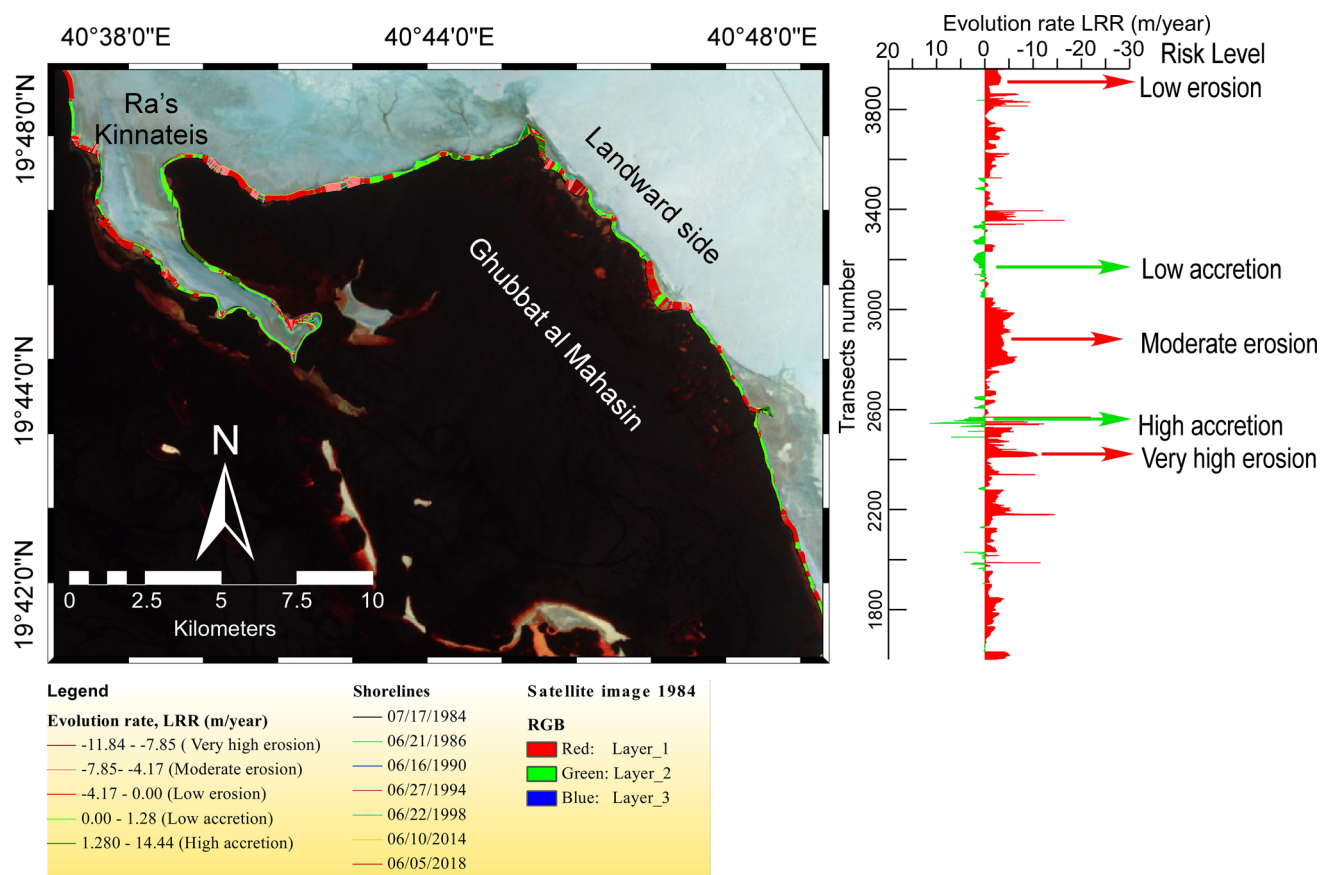


Fig. 8 Assessments of shorelines evolution along Ghubbat al Mahasin and Ra's Kinnateis

appropriate solutions to protect socio-environmental activities. One appropriate solution recommended by the authors was to take advantage of the acute erosion energy along the coast through constructing a nontraditional wave energy converter seawall, feeding nearby Al Lith City, and close by urbanizations with pure electricity.

Prediction Model

Shoreline evolution rates were utilized to brief historical shoreline developments and their futuristic forecast. Previously, few strategies have been utilized to forecast shoreline location as a temporal function, the rate of disintegration and accretion or rising sea level, for example, nonlinear mathematical models (e.g., cyclic arrangement models, an exponential model, and higher-order polynomial) (Li et al. 2001). Among them, endpoint rate and linear regression were considered as the most straightforward and helpful models (Nandi et al. 2016; Mondal et al. 2017; Nassar et al. 2018; San and Ulusar 2018). The EPR model has depended on presumption, which noticed the historical evolution rate, was best to evaluate accessible for prognosticating future without needing any other data such as waves, currents, tides, sea breeze, or a sediment supply

(Fenster et al. 1993). Future shorelines prognostication from satellite datasets for several intervals, utilizing this model is subject to a few affecting components like the exactness of shoreline discovery (precision of satellite information and technique utilized), the period of shoreline information obtaining, many data points taken into account over the designate of shoreline location and temporal changeability of shoreline and so forth (Galgano and Douglas 2000; Maiti and Bhattacharya 2009).

In the current study, the prediction models for short scale 2022 and long scale 2038 have been carried out using the EPR model based on extracted shorelines of 1984 and 2018 due to a significant positive relationship between EPR and LRR ($r^2 = 0.85$) (Fig. 6b). The extracted shoreline of 1984 is selected as the historical position, and the extracted shoreline of 2018 is utilized as the recent position for the predicted model. The results show that the shoreline position continues shifting land word, and broadly erosion took place in most of the portions of the investigation area. The scenario of these shifting is presented in Fig. 10, and the effectiveness of the prediction is described below.

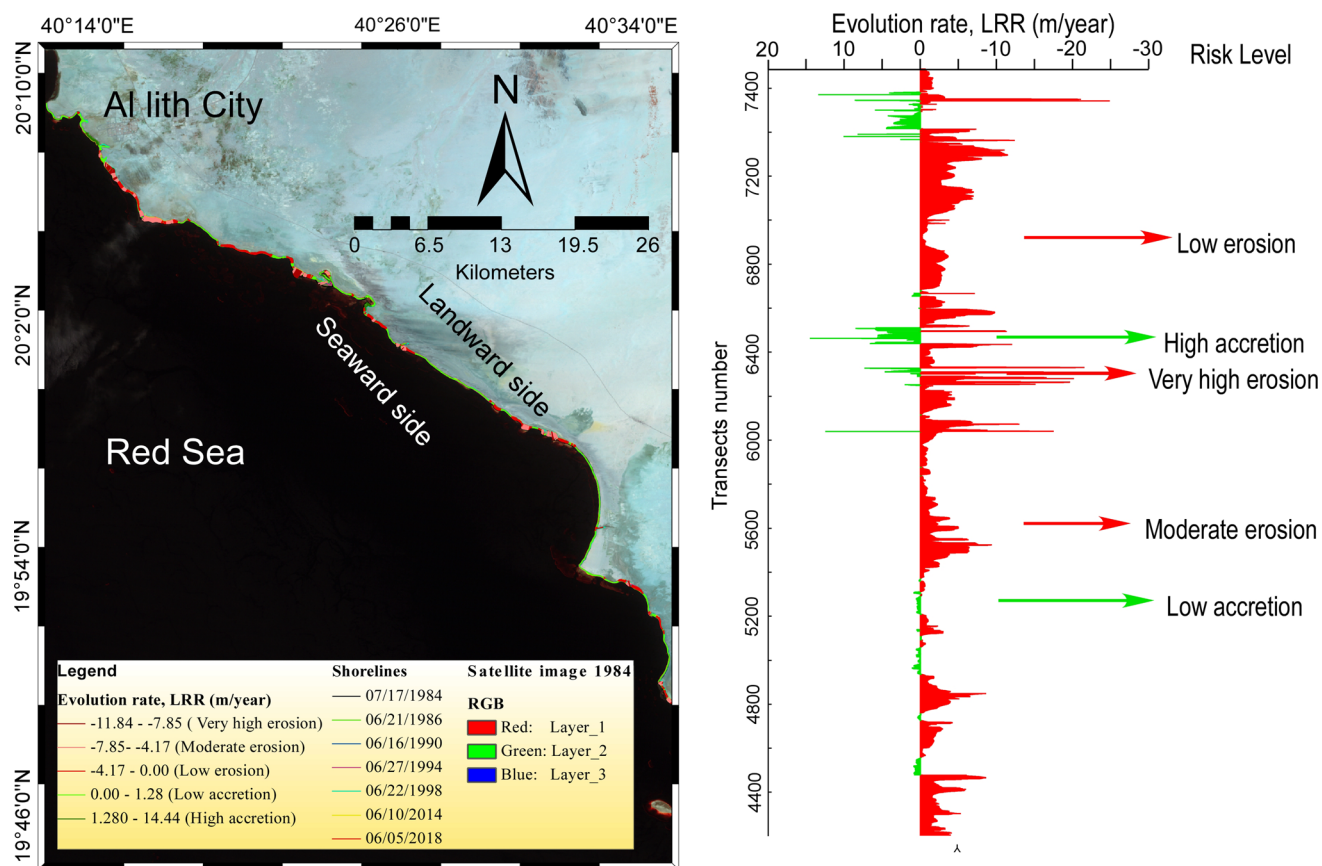


Fig. 9 Assessments of shorelines evolution between Al Lith and Ra's Kinnateis

Effectiveness of Prediction Model

The effectiveness of the prediction model was performed using the shifting of predicted shorelines of 1998 and 2017 by Eq. (1) to the extracted shorelines of 1998 and 2017 by TCT. Where, the predicted shorelines of 1998 and 2017 were based on the EPR for the years 1984–1996 and 1998–2014 across multiple transects with a distance of 20 m from the baseline. The abnormality position between predicted and extracted shorelines was analyzed by DSAS on 7706 transects with 20 m distance to the baseline and presented in Fig. 11. After that, the NRMSE was computed by Eq. (2). The NRMSE values were 0.26 and 0.24 for the years 1998 and 2017, respectively (Fig. 11a). These values indicate that EPR was an acceptable tool to predict futuristic shoreline for the study area. The futuristic positions of shoreline for short scale (4 years interval in 2022) and long scale (20 years interval in 2038) were forecasted based on Eq. (1). Around twenty transects are presented in Fig. 4 and Table 2 to show examples of the results.

Predictable Evolution Rate and Alteration Error

An error alteration operation has been applied in the futuristic shoreline prognostication fashion, depending upon shifting of predicted shorelines 1998 and 2017. The highest was in the southern part of the study area. The values of these errors were altered in the predicted shoreline positions of the short scale 2022 and long scale 2038. The results revealed that there was a slight decrease in the accretion and erosion as compared to normal prediction.

The predictable evolution rates (EPR) for the predicted shoreline (2018–2038) were graphically presented together with the evolution rate between the historical shorelines of 1984 and 2018 located from the south of Ras Mahasin Beach to the north of Al Lith Beach (Fig. 11b). This graph indicates that large portions of the coastal zones will continue to be vulnerable to high rates of shoreline disintegration. The continuance of this degradation will probably impact the environmental ecosystem, such as mangrove biozones and socio-environmental activities along the study area in the future if appropriate protection measures are not established.

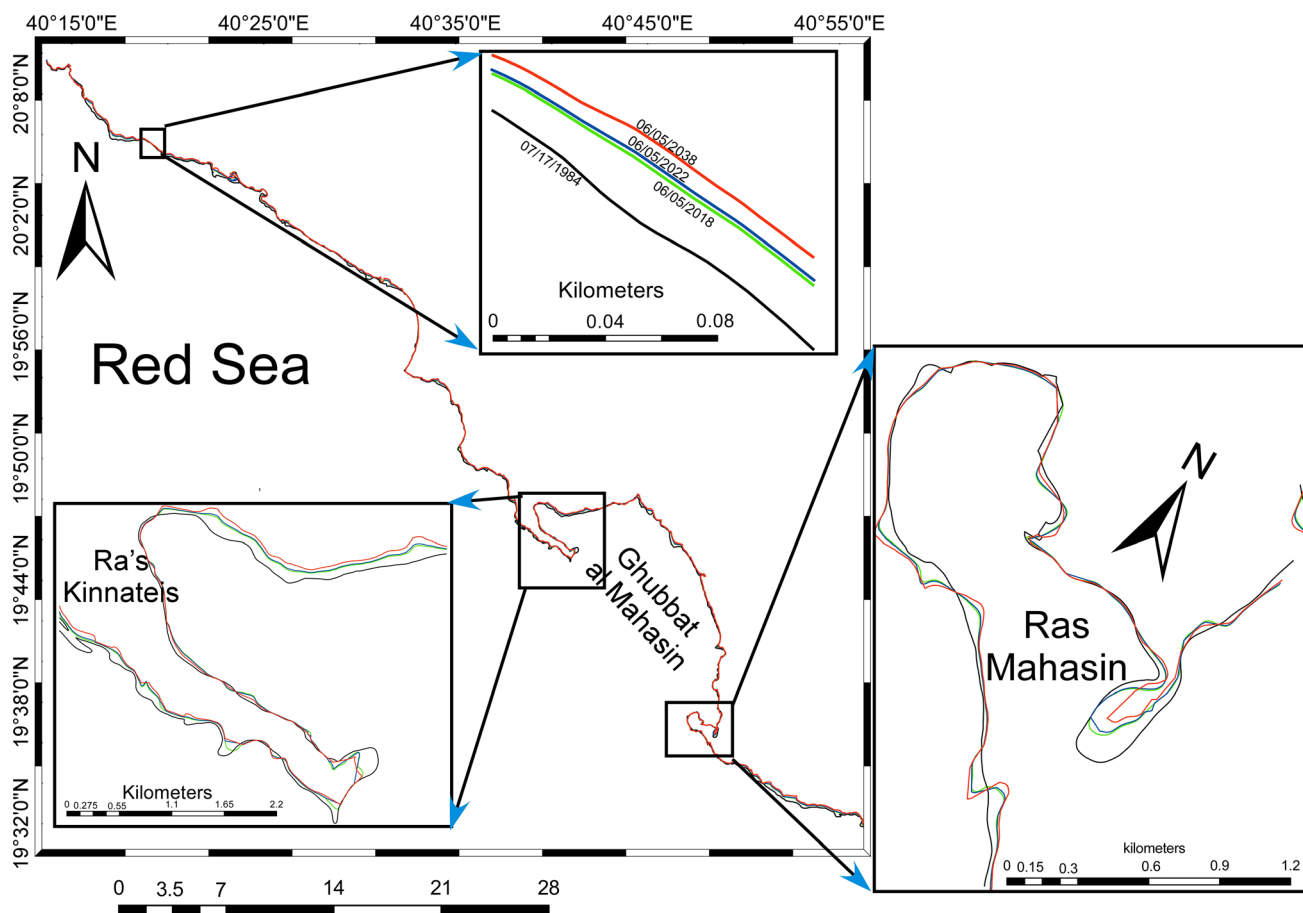


Fig. 10 Shoreline prediction for short scale 2022 and long scale 2038

Conclusions

Shoreline evolution between Al Lith and Ras Mahasin on the Red Sea coast, Saudi Arabia was effectively demarcated and analyzed between 1984 and 2018 frames, utilizing GIS techniques and automatic computations using DSAS. Shoreline evolution detection was widely explored along the coastal stretch utilizing multi-temporal satellite images over 34 years (between 1984 and 2018). Seven shoreline positions were extracted in 1984, 1986, 1990, 1994, 1998, 2014, and 2018 using the TCT technique. The investigation demonstrated a massive erosion process taking place in the investigated area. Chiefly, southern parts around marine heads have experienced high rates of disintegration. Growth was noticed in just a little bit of the northern part. Different reasons were attributed to the disintegration of the study area, such as the impact of the extreme wave action, the littoral drifts of sediments by

longshore current and windy storms. The massive erosion along the coastline of the investigation area indicated that the position of shoreline was more dynamics, which needed more attention and put appropriate solutions to protect socio-environmental activities.

On the other hand, the futuristic shoreline of the investigation area was prognosticated utilizing EPR for short scale 2022 and long scale 2038. However, some difficulties were found to achieve any perfection model. Ultimately, the prediction model revealed that the shoreline position will continue to shift landward in the future. Furthermore, the current study recommends decision-makers in the management of the coastal zone to exploit the massive erosion energy along the coastline for human activities as well as in the nearby cities, such as exploitation of the wave energy in this region to produce pure electrical energy.

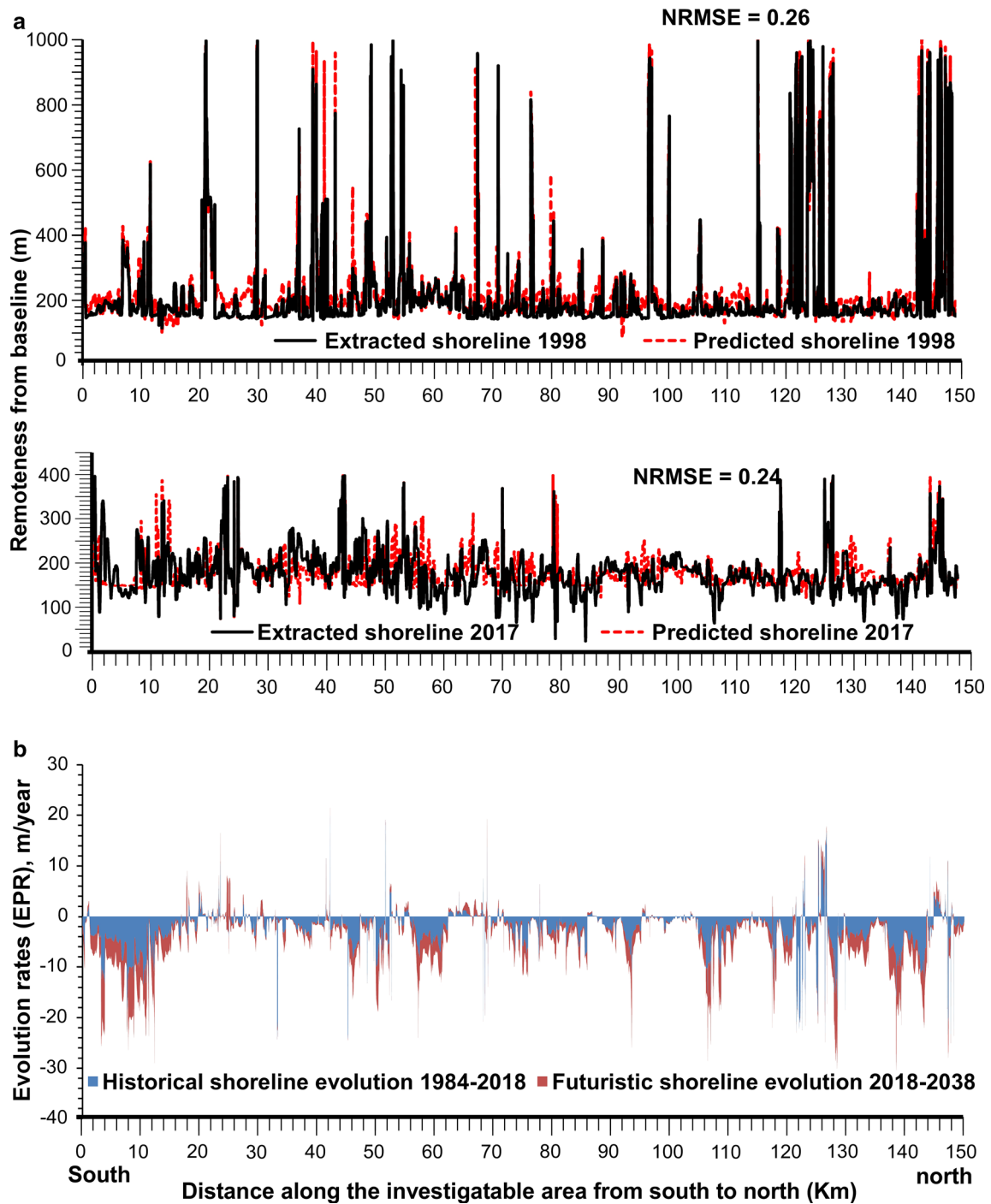


Fig. 11 a The abnormality between the predicted and extracted shorelines 2017 at each transect utilizing EPR with RMSE error. **b** The predictable evolution rates as EPR along the area of study

Table 2 Some examples for the estimation of predicted shoreline in 2022 and 2038 utilizing EPR prediction depend on Eq. (1)

Transect (ID)	Historical shoreline locations (remoteness from baseline, m)							mEPR (m/year)	Predicted shoreline locations (remoteness from baseline, m)	
	L_{1984}	L_{1986}	L_{1990}	L_{1994}	L_{1998}	L_{2014}	L_{2018}		L_{2022}	L_{2038}
1	243.8	236.5	213.2	229.6	165.0	172.0	181.1	- 1.9	173.7	144.1
2	252.4	245.2	220.8	237.2	172.5	181.8	189.8	- 1.9	182.4	152.8
3	261.0	253.1	228.5	244.2	180.0	191.7	198.3	- 1.9	190.9	161.3
4	269.6	259.6	236.1	251.0	187.1	201.6	206.8	- 1.9	199.4	169.8
5	279.0	265.2	244.3	257.7	194.3	210.7	214.9	- 1.9	207.4	177.1
6	289.7	271.1	253.1	264.6	201.7	218.2	221.9	- 2.0	213.9	181.9
7	304.4	279.9	262.5	272.8	209.0	225.4	228.6	- 2.2	219.6	183.8
8	325.1	292.6	272.1	281.6	215.5	232.6	235.8	- 2.6	225.2	183.0
9	346.6	315.6	283.5	290.5	222.1	240.6	243.8	- 3.0	231.6	183.2
10	366.4	333.8	296.7	301.8	229.1	249.1	253.4	- 3.3	240.0	186.6
11	384.3	352.1	309.8	314.4	237.5	257.4	263.4	- 3.6	249.1	192.0
12	400.2	370.6	322.7	327.5	246.9	264.0	272.3	- 3.8	257.2	196.7
13	414.3	384.9	334.9	340.5	256.2	269.2	278.9	- 4.0	263.0	199.1
14	427.8	399.1	347.4	352.7	263.8	273.3	283.0	- 4.3	265.9	197.4
15	441.4	405.5	360.7	365.7	268.8	274.8	285.5	- 4.6	267.1	193.5
16	455.0	407.8	374.3	380.0	270.8	273.2	285.7	- 5.0	265.7	185.7
17	467.2	421.7	387.6	394.4	270.4	268.7	284.6	- 5.4	263.1	176.8
18	477.1	442.4	398.7	408.7	267.2	260.2	280.6	- 5.8	257.4	164.6
19	484.0	452.6	406.9	421.7	260.8	248.5	274.9	- 6.2	250.2	151.5
20	487.4	462.6	411.7	432.4	250.6	234.3	265.1	- 6.6	238.8	133.9

Acknowledgments This work was supported by the deanship of Scientific Research (DSR), King Abdulaziz University, Jeddah, under Grant No. (DG-1440-22-1440-150). The authors, therefore, gratefully acknowledge the DSR technical and financial support. The authors are very grateful for the editor and reviewers for their constructive comments and editorial handling.

References

- Aboobacker, V. M., Shanas, P. R., Alsaafani, M. A., & Albarakati, A. M. A. (2017). Wave energy resource assessment for Red Sea. *Renewable Energy*, 114, 46–58. <https://doi.org/10.1016/j.renene.2016.09.073>.
- Aboulela, H. A., Bantan, R. A., & Zeineldin, R. A. (2020). Evaluating and predicting changes occurring on the coastlines of Jeddah city using satellite images. *Arabian Journal for Science and Engineering*, 45, 327–339.
- Abu-Zied, R. H., & Bantan, R. A. (2015). Palaeoenvironment, palaeoclimate and sea-level changes in the Shuaiba Lagoon during the late Holocene (last 3.6 ka), eastern Red Sea coast, Saudi Arabia. *The Holocene*, 25, 1301–1312.
- Addo, K. A., Jayson-Quashigah, P. N., & Kufogbe, K. S. (2012). Quantitative analysis of shoreline change using medium resolution satellite imagery in Keta, Ghana. *Marine Science*, 1, 1–9. <https://doi.org/10.5923/j.ms.20110101.01>.
- Addo, K. A., Walkden, M., & Mills, J. P. (2008). Detection, measurement and prediction of shoreline recession in Accra, Ghana. *ISPRS Journal of Photogrammetry and Remote Sensing*, 63, 543–558. <https://doi.org/10.1016/j.isprsjprs.2008.04.001>.
- Aedla, R., Dwarakish, G. S., & Reddy, D. V. (2015). Automatic shoreline detection and change detection analysis of Netravati-GurpurRivermouth using histogram equalization and adaptive thresholding techniques. *Aquatic Procedia*, 4, 563–570. <https://doi.org/10.1016/j.aqpro.2015.02.073>.
- Alharbi, O. A., Phillips, M. R., Williams, A. T., & Bantan, R. A. (2011). Landsat ETM applications: Identifying geological and coastal landforms, SE Red Sea coast, Saudi Arabia. *Medcoast*, 11, 985.
- Alharbi, O. A., Phillips, M. R., Williams, A. T., Thomas, T., Hakami, M., Kerbe, J., et al. (2017). Temporal shoreline change and infrastructure influences along the southern Red Sea coast of Saudi Arabia. *Arabian Journal of Geosciences*. <https://doi.org/10.1007/s12517-017-3109-7>.
- Almonacid-Caballer, J., Sánchez-García, E., Pardo-Pascual, J. E., Balaguer-Beser, A. A., & Palomar-Vázquez, J. (2016). Evaluation of annual mean shoreline position deduced from Landsat imagery as a mid-term coastal evolution indicator. *Marine Geology*, 372, 79–88. <https://doi.org/10.1016/j.margeo.2015.12.015>.
- AL-Sheikh, A. B. Y. (2012). Environmental degradation and its impact on tourism in Jazan, KSA using remote sensing and GIS. *International Journal of Environmental Sciences*, 3, 421–432.
- Al-zubieri, A. G., Bantan, R. A., Abdalla, R., Antoni, S., Al-Dubai, T. A., & Majeed, J. (2018). Application of GIS and remote sensing to monitor the impact of development activities on the coastal zone of Jazan City on the Red Sea, Saudi Arabia. *International Archives of the Photogrammetry, Remote Sensing and Spatial*

- Information Sciences*. <https://doi.org/10.5194/isprs-archives-XLII-3-W4-45-2018>.
- Bantan, R. (1999). *Geology and sedimentary environments of Farasan Bank (Saudi Arabia), southern Red Sea: A combined remote sensing and field study*.
- Baral, R., Pradhan, S., Samal, R. N., & Mishra, S. K. (2018). Shoreline change analysis at Chilika Lagoon Coast, India using digital shoreline analysis system. *Journal of the Indian Society of Remote Sensing*, 46, 1637–1644. <https://doi.org/10.1007/s12524-018-0818-7>.
- Behairy, A. K. A., Rao, N. V. N. D., & El-Shater, A. (1991). A siliciclastic coastal sabkha, Red Sea coast, Saudi Arabia. *Marine Sciences*, 2, 65–77.
- Bheeroo, R. A., Chandrasekar, N., Kaliraj, S., & Magesh, N. S. (2016). Shoreline change rate and erosion risk assessment along the Trou Aux Biches-Mont Choisy beach on the northwest coast of Mauritius using GIS-DSAS technique. *Environmental Earth Sciences*, 75, 1–12. <https://doi.org/10.1007/s12665-016-5311-4>.
- Boak, E. H., & Turner, I. L. (2005). Shoreline definition and detection: A review. *Journal of coastal research*, 21, 688–703.
- Castelle, B., Guillot, B., Marieu, V., Chaumillon, E., Hanquiez, V., Bujan, S., et al. (2018). Spatial and temporal patterns of shoreline change of a 280-km high-energy disrupted sandy coast from 1950 to 2014: SW France. *Estuarine, Coastal and Shelf Science*, 200, 212–223. <https://doi.org/10.1016/j.ecss.2017.11.005>.
- Ciritci, D., & Türk, T. (2019). Automatic detection of shoreline change by geographical information system (GIS) and remote sensing in the Göksu Delta, Turkey. *Journal of the Indian Society of Remote Sensing*, 47, 233–243. <https://doi.org/10.1007/s12524-019-00947-1>.
- Ciritci, D., & Turk, T. (2020). Assessment of the Kalman filter-based future shoreline prediction method. *International Journal of Environmental Science and Technology*, 17, 3801–3816.
- Edwards, F. J. (1987). Climate and oceanography. *Red sea*, 1, 45–68.
- El-Sharmouby, B. A., El-Alfy, K. S., Rageh, O. S., & El-Sharabasy, M. M. (2015). Coastal changes along Gamasa beach, Egypt. *Journal of Coastal Zone Management*, 17, 393.
- Fan, Y., Chen, S., Zhao, B., Pan, S., Jiang, C., & Ji, H. (2018). Shoreline dynamics of the active Yellow River delta since the implementation of Water-Sediment Regulation Scheme. A remote-sensing and statistics-based approach. *Estuarine, Coastal and Shelf Science*, 200, 406–419. <https://doi.org/10.1016/j.ecss.2017.11.035>.
- Fenster, M. S., Dolan, R., & Elder, J. F. (1993). A new method for predicting shoreline positions from historical data. *Journal of Coastal Research*, 9, 147–171.
- Galgano, F. A., & Douglas, B. C. (2000). Shoreline position prediction: methods and errors. *Environmental Geosciences*, 7, 23–31.
- Genz, A. S., Fletcher, C. H., Dunn, R. A., Frazer, L. N., & Rooney, J. J. (2007). The predictive accuracy of shoreline change rate methods and alongshore beach variation on Maui, Hawaii. *Journal of Coastal Research*, 23, 87–105.
- Gharbi, S. H., Albarakati, A. M., Alsaafani, M. A., Saheed, P. P., & Alraddadi, T. M. (2018). Simulation of tidal hydrodynamics in the Red Sea using COHERENS model. *Regional Studies in Marine Science*, 22, 49–60.
- Hagenaars, G., de Vries, S., Luijendijk, A. P., de Boer, W. P., & Reniers, A. J. H. M. (2018). On the accuracy of automated shoreline detection derived from satellite imagery: A case study of the sand motor mega-scale nourishment. *Coastal Engineering*, 133, 113–125. <https://doi.org/10.1016/j.coastaleng.2017.12.011>.
- Holland, K. T., & Elmore, P. A. (2008). A review of heterogeneous sediments in coastal environments. *Earth-Science Reviews*, 89, 116–134.
- Huang, C., Wylie, B., Yang, L., Homer, C., & Zylstra, G. (2002). Derivation of a tasselled cap transformation based on Landsat 7 at-satellite reflectance. *International Journal of Remote Sensing*, 23, 1741–1748.
- Jonah, F. E., Boateng, I., Osman, A., Shimba, M. J., Mensah, E. A., Adu-Boahen, K., et al. (2016). Shoreline change analysis using end point rate and net shoreline movement statistics: An application to Elmina, Cape Coast and Moree section of Ghana's coast. *Regional Studies in Marine Science*, 7, 19–31. <https://doi.org/10.1016/j.rsma.2016.05.003>.
- Kabuth, A. K., Kroon, A., & Pedersen, J. B. T. T. (2014). Multidecadal shoreline changes in Denmark. *Journal of Coastal Research*, 30, 714–728. <https://doi.org/10.2112/JCOASTRES-D-13-00139.1>.
- Li, R., Liu, J.-K., & Felus, Y. (2001). Spatial modeling and analysis for shoreline change detection and coastal erosion monitoring. *Marine Geodesy*, 24, 1–12.
- Maanan, M., Ruiz-Fernandez, A. C., Maanan, M., Fattal, P., Zourarah, B., & Sahabi, M. (2014). A long-term record of land use change impacts on sediments in Oualidia lagoon, Morocco. *International Journal of Sediment Research*, 29, 1–10.
- Mahapatra, M., Ramakrishnan, R., & Rajawat, A. S. (2015). Coastal vulnerability assessment using analytical hierarchical process for South Gujarat coast, India. *Natural Hazards*, 76, 139–159. <https://doi.org/10.1007/s11069-014-1491-y>.
- Mahapatra, M., Ratheesh, R., & Rajawat, A. S. (2014). Shoreline change analysis along the coast of South Gujarat, India, using digital shoreline analysis system. *Journal of the Indian Society of Remote Sensing*, 42, 869–876. <https://doi.org/10.1007/s12524-013-0334-8>.
- Maiti, S., & Bhattacharya, A. K. (2009). Shoreline change analysis and its application to prediction: A remote sensing and statistics based approach. *Marine Geology*, 257, 11–23.
- May, V. J., & Hansom, J. D. (2003). Coastal geomorphology of Great Britain. *Joint Nature Conservation Committee*, 28.
- Mondal, I., Bandyopadhyay, J., & Dhara, S. (2017). Detecting shoreline changing trends using principle component analysis in Sagar Island, West Bengal, India. *Spatial Information Research*, 25, 67–73.
- Mukhopadhyay, A., Mukherjee, S., Mukherjee, S., Ghosh, S., Hazra, S., & Mitra, D. (2012). Automatic shoreline detection and future prediction: A case study on Puri Coast, Bay of Bengal, India. *European Journal of Remote Sensing*, 45, 201–213.
- Murali, R. M., Dhiman, R., Choudhary, R., Seelam, J. K., Ilangoan, D., & Vethamony, P. (2015). Decadal shoreline assessment using remote sensing along the central Odisha coast, India. *Environmental Earth Sciences*, 74, 7201–7213.
- Murray, S. P., & Johns, W. (1997). Direct observations of seasonal exchange through the Bab el Mandab Strait. *Geophysical Research Letters*, 24, 2557–2560.
- Nandi, S., Ghosh, M., Kundu, A., Dutta, D., & Baksi, M. (2016). Shoreline shifting and its prediction using remote sensing and GIS techniques: A case study of Sagar Island, West Bengal (India). *Journal of coastal conservation*, 20, 61–80.
- Nassar, K., Fath, H., Mahmud, W. E., Masria, A., Nadaoka, K., & Negm, A. (2018). Automatic detection of shoreline change: case of North Sinai coast, Egypt. *Journal of Coastal Conservation*. <https://doi.org/10.1007/s11852-018-0613-1>.
- Nofal, R., & Abboud, I. A. (2016). Geomorphological evolution of marine heads on the eastern coast of Red Sea at Saudi Arabian region, using remote sensing techniques. *Arabian Journal of Geosciences*, 9, 1–15. <https://doi.org/10.1007/s12517-015-2234-4>.
- Pardo-Pascual, J. E., Almonacid-Caballer, J., Ruiz, L. A., & Palomar-Vázquez, J. (2012). Automatic extraction of shorelines from Landsat TM and ETM+ multi-temporal images with subpixel

- precision. *Remote Sensing of Environment*, 123, 1–11. <https://doi.org/10.1016/j.rse.2012.02.024>.
- Pianca, C., Holman, R., & Siegle, E. (2015). Shoreline variability from days to decades: Results of long-term video imaging. *Journal of Geophysical Research: Oceans*, 120, 2159–2178.
- Qiao, G., Mi, H., Wang, W., Tong, X., Li, Z., Li, T., et al. (2018). 55-year (1960–2015) spatiotemporal shoreline change analysis using historical DISP and Landsat time series data in Shanghai. *International Journal of Applied Earth Observation and Geoinformation*, 68, 238–251. <https://doi.org/10.1016/j.jag.2018.02.009>.
- Rabehi, W., Guerfi, M., Mahi, H., & Rojas-Garcia, E. (2019). Spatiotemporal monitoring of coastal urbanization dynamics: Case study of Algiers' Bay, Algeria. *Journal of the Indian Society of Remote Sensing*, 47, 1917–1936.
- Ralston, D. K., Jiang, H., & Farrar, J. T. (2013). Waves in the Red Sea: Response to monsoonal and mountain gap winds. *Continental Shelf Research*, 65, 1–13. <https://doi.org/10.1016/j.csr.2013.05.017>.
- San, B. T., & Ulusar, U. D. (2018). An approach for prediction of shoreline with spatial uncertainty mapping (SLiP-SUM). *International Journal of Applied Earth Observation and Geoinformation*, 73, 546–554. <https://doi.org/10.1016/j.jag.2018.08.005>.
- Shetty, A., Jayappa, K. S., Ramakrishnan, R., & Rajawat, A. S. (2019). Shoreline dynamics and vulnerability assessment along the Karnataka Coast, India: A geo-statistical approach. *Journal of the Indian Society of Remote Sensing*, 47, 1223–1234. <https://doi.org/10.1007/s12524-019-00980-0>.
- Siddall, M., Rohling, E. J., Almogi-Labin, A., Hemleben, C., Meischner, D., Schmelzer, I., et al. (2003). Sea-level fluctuations during the last glacial cycle. *Nature*, 423, 853.
- Taqi, A. M., Al-Subhi, A. M., Alsaafani, M. A., & Abdulla, C. P. (2019). estimation of geostrophic current in the Red Sea based on sea level anomalies derived from extended satellite altimetry data. *Ocean Science*, 15, 477–488.
- Thieler, E. R., Himmelstoss, E. A., Zichichi, J. L., & Ergul, A. (2009). The digital shoreline analysis system (DSAS) version 4.0-an ArcGIS extension for calculating shoreline change. US Geological Survey.
- Tran Thi, V., Tien Thi Xuan, A., Phan Nguyen, H., Dahdouh-Guebas, F., & Koedam, N. (2014). Application of remote sensing and GIS for detection of long-term mangrove shoreline changes in Mui Ca Mau, Vietnam. *Biogeosciences*, 11, 3781–3795.
- Vousdoukas, M. I., Ranasinghe, R., Mentaschi, L., Plomaritis, T. A., Athanasiou, P., Luijendijk, A., et al. (2020). Sandy coastlines under threat of erosion. *Nature Climate Change*, 10, 260–263. <https://doi.org/10.1038/s41558-020-0697-0>.
- Zhang, X., Yang, Z., Zhang, Y., Ji, Y., Wang, H., Lv, K., et al. (2018). Spatial and temporal shoreline changes of the southern Yellow River (Huanghe) Delta in 1976–2016. *Marine Geology*, 395, 188–197. <https://doi.org/10.1016/j.margeo.2017.10.006>.

Publisher's Note Springer Nature remains neutral with regard to jurisdictional claims in published maps and institutional affiliations.